

Distance scale for high-luminosity stars in OB associations and in field with *Gaia* DR2. Spurious systematic motions

A. M. Melnik* • A. K. Dambis

Abstract

We calculated the median parallaxes for 47 OB associations including at least 10 stars with known *Gaia* DR2 parallaxes. A comparison between trigonometric and photometric parallaxes of OB associations reveals a zero-point offset of $\Delta\varpi = -0.11 \pm 0.04$ mas indicating that *Gaia* DR2 parallaxes are, on average, underestimated and the distances derived from them are overestimated. The correction of $\Delta\varpi = -0.11$ mas is consistent with the estimate that Arenou et al. (2018) obtained for bright stars. An analysis of parallaxes of OB associations and high-luminosity field stars confirms our previous conclusion (Dambis et al. 2001) that the distance scale for OB stars established by Blaha and Humphreys (1989) must be reduced by 10–20%. Spurious systematic motions of 10–20 km s^{−1} at the distances of 2–3 kpc from the Sun are found to arise from the use of the uncorrected *Gaia* DR2 parallaxes.

Keywords Galaxy: open clusters and associations: general; parallaxes; proper motions; Galaxy: kinematics and dynamics

1 Introduction

The second intermediate *Gaia* data release (*Gaia* DR2) includes high-precision proper motions and parallaxes for 1.3 billion stars (Gaia Collaboration et al. 2018a; Lindegren et al. 2018a), which open up new possibilities for the study of the Galactic structure and kinematics (Gaia Collaboration et al. 2018b;

Fragkoudi et al. 2019; Carrillo et al. 2019; Hunt et al. 2019; Pettitt, Ragan & Smith 2020, and other papers).

The Hipparcos (ESA 1997) and *Gaia* (Gaia Collaboration et al. 2016) satellites have the possibility to measure the absolute parallaxes, but this capability is susceptible to various instrumental effects, especially to the basic-angle variations. The basic angle monitor (BAM) effectively corrects the changes of the basic angle but the remaining small variations cannot be removed (Lindegren et al. 2018a).

Many researchers investigated the zero-point bias, $\Delta\varpi$, of *Gaia* DR2 parallaxes but different studies give different zero-point corrections. Lindegren et al. (2018a) derived $\Delta\varpi = -0.029 \pm 0.002$ mas, which means that *Gaia* parallaxes are systematically underestimated and must be increased by 0.029 mas, i.e. distances for all *Gaia* DR2 stars must be decreased. Stassun & Torres (2018) compared the parallaxes of eclipsing binaries with *Gaia* DR2 parallaxes and found a systematic difference of $\Delta\varpi = -0.082 \pm 0.33$ mas. Zinn et al. (2019) obtained the zero-point offset equal to $\Delta\varpi = -0.053 \pm 0.003$ mas using stars from the red giant branch. Riess et al. (2018) found the offset to be $\Delta\varpi = -0.046 \pm 0.013$ mas from an analysis of bright Cepheids. Leung & Bovy (2019) compared spectro-photometric parallaxes of APOGEE stars to *Gaia* DR2 parallaxes and obtained a zero point bias of $\Delta\varpi = -0.052 \pm 0.002$ mas. A parallax correction close to -0.05 mas is found in many other studies (Yalyalieva et al. 2018; Schönrich, McMillan & Eyer 2019).

Moreover, there is evidence that the zero-point offset depends on the stellar color and magnitude (Zinn et al. 2019; Arenou et al. 2018; Leung & Bovy 2019). Arenou et al. (2018, Table 1) compared *Gaia* DR2 parallaxes with other catalogs and determined the zero-point difference in parallaxes for different samples of stars. Their analysis reveals a dependence between

A. M. Melnik

A. K. Dambis

Sternberg Astronomical Institute, Lomonosov Moscow State University, Universitetskij pr. 13, Moscow 119991, Russia

* e-mail: anna@sai.msu.ru

the zero-point offset $\Delta\varpi$ and the average G-band magnitude of stars in the catalog: the brighter the stars the larger the absolute value of the zero-point offset, $|\Delta\varpi|$.

OB associations are sparse groups of O- and B-type stars (for example, Ambartsumian 1949; Blaauw 1964). In this paper we study the zero-point bias in parallaxes for OB associations and high-luminosity field stars with photometric distance scale established by Blaha & Humphreys (1989), derive the rotation curve from *Gaia* DR2 data, and study the systematic non-circular motions. Section 2 describes the kinematical data for stars of OB associations and high-luminosity field stars. In Section 3 we compare the photometric and trigonometric parallaxes, study the distance scale and the Galactic rotation curve, presents the systematic motions calculated for different distance scales. Section 4 discusses the results and formulates main conclusions.

2 Data

The catalog of Galactic high-luminosity stars by Blaha & Humphreys (1989) includes two parts: stars in OB associations and stars scattered in the field. Both catalogs present photometric data for main-sequence O–B2-type stars, bright giants of spectral types O–B3, and supergiants of all spectral types. Note that the fraction of red supergiants of spectral types K and M is only 5% in both catalogs. The catalog of stars in OB associations contains 2209 stars of 91 OB associations located within ~ 3 kpc from the Sun. The catalog of high-luminosity field stars includes 2492 objects which do not show the concentration to any groups. Blaha & Humphreys (1989) derive the distances to OB associations and to field stars, r_{bh} , on the basis of their spectral types and luminosity classes. Stars of both catalogs are massive young stars and their ages do not exceed 40 Myr (Bressan et al. 2012).

We supplemented the catalogs by Blaha & Humphreys (1989) with kinematical data for high-luminosity stars. We cross-matched both catalogs with the *Gaia* DR2 data to search for precise proper motions and parallaxes, which we found for $\sim 90\%$ of stars. Only 7% of stars from the list by Blaha & Humphreys (1989) have line-of-sight velocities, V_r , measured by the *Gaia* spectrometer, so here we use the velocities V_r from the catalog by Barbier-Brossat & Figon (2000), which are available for 52% of stars of both catalogs.

In this paper we use the refined sample of stars in OB associations and high-luminosity field stars which includes only stars with the re-normalised unit weight errors (RUWE) less than $\text{RUWE} < 1.4$ and with the

number of visibility periods $n_{vis} > 8$ (Arenou et al. 2018; Lindegren et al. 2018a; Lindegren 2018). The refined sample of stars in OB associations includes 1771 stars with $n_{vis} > 8$ and $\text{RUWE} < 1.4$; of 219 excluded stars, 174 stars have $\text{RUWE} \geq 1.4$ and 45 objects have $n_{vis} \leq 8$.

We described the catalog of stars of OB associations in our previous papers (Melnik & Dambis 2017, 2020). Here we give the description of the second part of the catalog of high-luminosity stars compiled by Blaha & Humphreys (1989). Of 2492 field stars 2340 (94%) are cross-matched with *Gaia* DR2 catalog and 2319 stars have *Gaia* DR2 proper motions and parallaxes. We excluded from the full sample 66 stars with $n_{vis} \leq 8$ and 164 stars with $\text{RUWE} \geq 1.4$. Thus, the refined sample of field stars contains 2089 objects. Table 1 (available in the online version of the paper) lists the kinematic and photometric data for high-luminosity stars in the field. It presents the name of a star, spectral type, luminosity class, color indices $B - V$ and $U - B$, apparent and absolute magnitudes, m_V and M_V , and the V -band extinction, A_V , that are adopted from the catalog by Blaha & Humphreys (1989). We present the heliocentric distance to the star by Blaha & Humphreys (1989), r_{bh} , reduced to the short distance scale, $r = 0.8r_{bh}$, which is consistent with the Berdnikov et al. (2000) distance scale for classical Cepheids (Sitnik & Melnik 1996; Dambis, Melnik & Rastorguev 2001; Melnik & Dambis 2009). The absolute magnitudes obtained by Blaha & Humphreys (1989), $M_{V(BH)}$, were converted to the short distance scale $M_V = M_{V(BH)} + \Delta m$, where $\Delta m = -5 \log 0.8 = 0.485^m$. Table 1 also lists *Gaia* DR2 data: equatorial coordinates, α and δ , of the star; its Galactic coordinates, l and b ; the G -band magnitude; the parallax, ϖ ; proper-motion components along l - and b -directions, μ_l and μ_b , and their errors, ε_ϖ , ε_{μ_l} and ε_{μ_b} ; the error RUWE and the number of visibility periods, n_{vis} . Table 1 also gives the line-of-sight velocities, V_r , and their errors, ε_{vr} , taken from the catalog by Barbier-Brossat & Figon (2000).

3 Results

3.1 Zero-point bias of the distance scale to OB associations

The trigonometric parallaxes to OB associations, ϖ_g , are determined as the median values of *Gaia* DR2 parallaxes of their member stars. We selected 47 OB associations including more than 9 stars with known *Gaia* DR2 parallaxes. The photometric parallaxes are

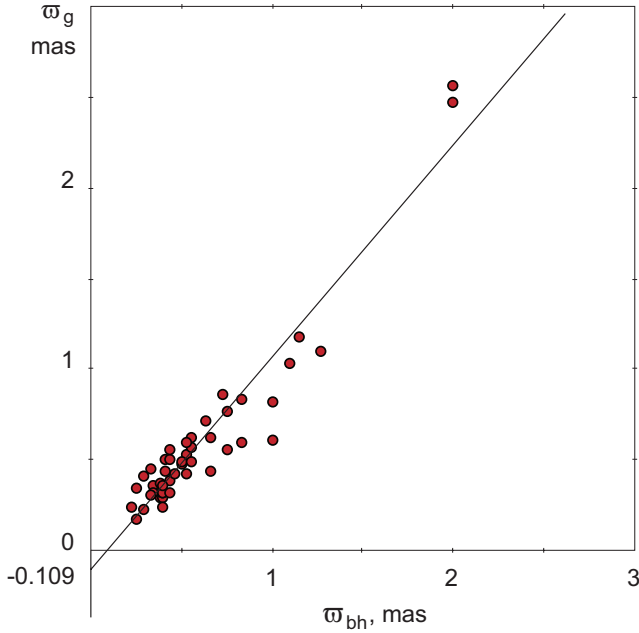


Fig. 1 Comparison between trigonometric, ϖ_g , and photometric, ϖ_{bh} , parallaxes of 47 OB associations. The straight line shows the linear dependence between these quantities, $\varpi_g = 1.16 \varpi_{bh} - 0.11$ mas. We can see that it does not pass through the origin but crosses the vertical axis at negative values, which is indicative of a systematic excess of photometric parallaxes over trigonometric parallaxes. Consequently, *Gaia* DR2 parallaxes must be increased, whereas the corresponding distances to OB associations must be reduced.

calculated as inverse values of the photometric distances, $\varpi_{bh} = 1/r_{bh}$, to OB associations derived by Blaha & Humphreys (1989). The least-squares solution of 47 linear equations:

$$\varpi_g = k_p \varpi_{bh} + \Delta\varpi \quad (1)$$

gives the most probable values of the coefficients equal to $k_p = 1.159 \pm 0.055$ and $\Delta\varpi = -0.109 \pm 0.039$ mas:

$$\varpi_g = (1.159 \pm 0.055) \varpi_{bh} - (0.109 \pm 0.039) \text{ mas}. \quad (2)$$

The root-mean-square deviation from the linear dependence appears to be 0.14 mas.

Figure 1 shows the distribution of trigonometric, ϖ_g , and photometric, ϖ_{bh} , parallaxes of 47 OB associations. The linear dependence between them determined by Eq. 2 is shown by the straight line. We can see that the straight line does not pass through the origin but crosses the vertical axis at the negative value of trigonometric parallaxes indicating a systematic excess of photometric parallaxes over trigonometric parallaxes. The systematic offset of trigonometric parallaxes over photometric parallaxes is determined mainly by distant objects located beyond 1 kpc from the Sun, $r > 1$ kpc. On the contrary, the coefficient of the distance scale is determined mainly by nearby objects, $r < 1$ kpc.

A comparison of trigonometric and photometric parallaxes requires some caution: they have different distributions of errors which can give rise to systematic errors (Luri et al. 2018). Note that the random error in photometric distances to OB associations (without the allowance for the uncertainty of the zero-point of the distance scale) is, on average, 6% (Melnik & Dambis 2009). We simulated the distribution of observational errors in photometric distances and trigonometric parallaxes and calculated the biases in parameters k_p and $\Delta\varpi$ caused by such errors. The distance modulus, $m_V - M_V$, of an object without correction for extinction is determined by the relation:

$$DM = 5 \lg r + 10, \quad (3)$$

where r is in kpc. Here we assume that the distance moduli of stars of OB association are obtained with a random error of 0.5^m , so the uncertainty in the distance modulus of an OB association must be equal to:

$$\sigma_m = 0.5^m / \sqrt{n_t}, \quad (4)$$

where n_t is the number of stars of the OB association with known photometry (see Table 3). The total errors

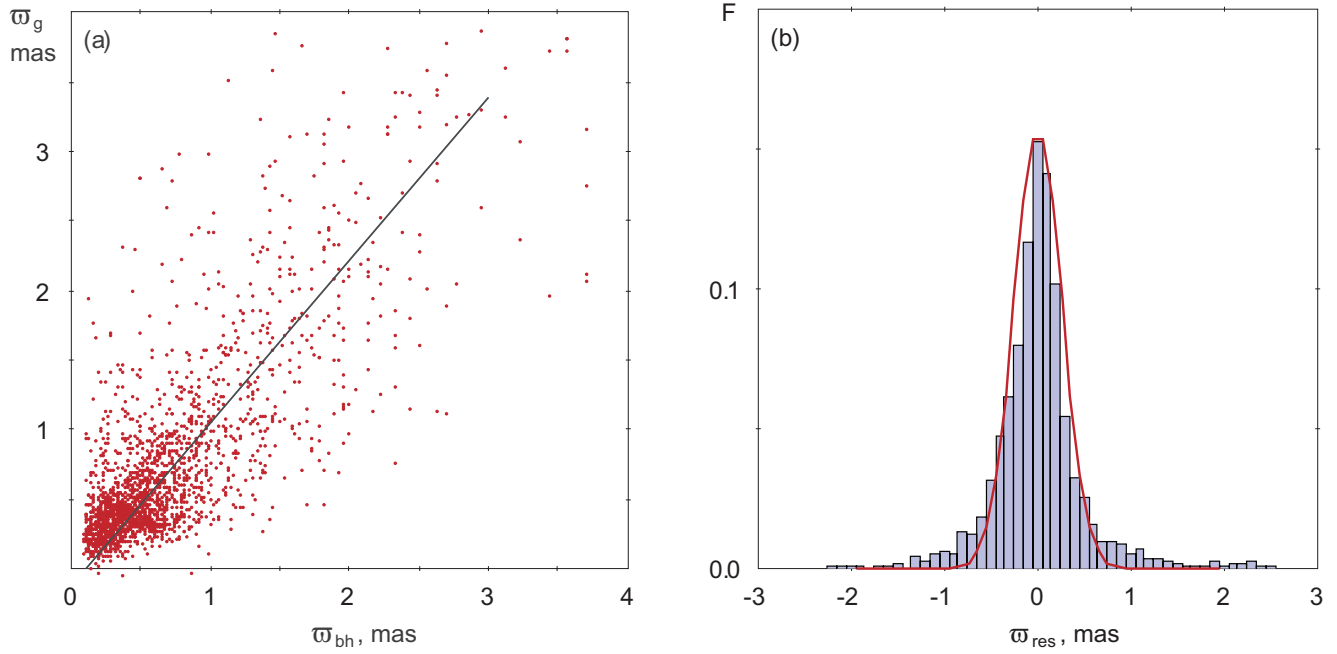


Fig. 2 (a) Trigonometric, ϖ_g , parallaxes plotted as a function of photometric, ϖ_{bh} , parallaxes for 2089 high-luminosity field stars. The straight line shows the linear dependence between these quantities (Eq. 10). The most probable value of k_p appears to be 1.16 ± 0.01 . (b) Distribution of the residual parallaxes, ϖ_{res} (Eq. 12). The solid curve shows the Gaussian distribution with the standard deviation of $\sigma = 0.26$ mas, which fits well the observed distribution in the central $\pm 2\sigma$ -interval.

in *Gaia* DR2 parallaxes are believed to be given by formula:

$$\sigma_p = \sqrt{k^2 \sigma_i^2 + \sigma_s^2}, \quad (5)$$

where σ_i is the formal uncertainty in a stellar parallax (possibly underestimated) and σ_s is the systematic error in parallaxes. The factor k and systematic error σ_s take different values for bright ($G < 13^m$) and faint ($G > 13^m$) stars. Note that the average G magnitude of stars of OB association from the catalog by Blaha & Humphreys (1989) is $\overline{G} = 8.5^m$. We therefore adopted the k and σ_s values equal to $k = 1.08$ and $\sigma_s = 0.021$ mas, respectively (Arenou et al. 2018; Lindegren et al. 2018a; Lindegren et al. 2018b).

We suppose that true values of ϖ_g and $\varpi_{bh} = 1/r_{bh}$ are connected through Eq. 2. As we do not know true values we use observational values instead of them. Here we implicitly assume that the distributions of true and wrong values are nearly the same. We simulated the observational errors in distance moduli $DM(r_{bh})$ (Eq. 3) of OB associations and in parallaxes ϖ_g by adding normally distributed values with the standard deviations determined by Eqs 4 and 5, respectively. Then we derived the parameters k_p and $\Delta\varpi$ from 'wrong' data. The calculated values, k'_p and $\Delta\varpi'$, of

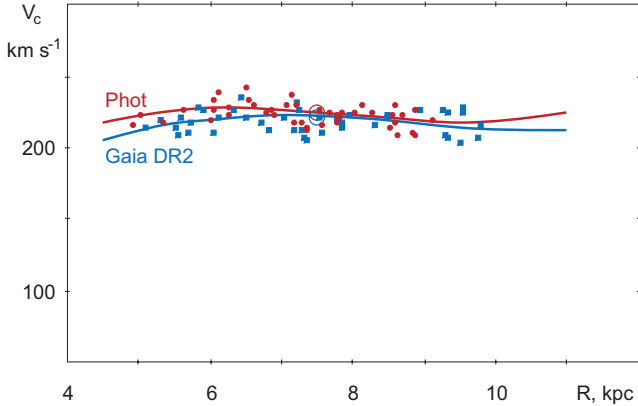


Fig. 3 Two rotation curves of the Galactic disk derived with the use of photometric and trigonometric distances to OB associations. The large circle indicates the position of the Sun. The azimuthal velocities of OB associations calculated with the use of photometric and trigonometric distances are indicated by circles and squares, respectively.

the parameters appear to be slightly different from the true ones, k_p^0 and $\Delta\varpi^0$. We modelled 10^3 observational samples and estimated the average values of systematic corrections:

$$k_p' - k_p^0 = -0.008, \quad (6)$$

$$\Delta\varpi' - \Delta\varpi^0 = 0.004, \text{ mas} \quad (7)$$

which must be subtracted from the calculated earlier values $k_p = 1.159$ and $\Delta\varpi = -0.109$ mas (Eq. 2). So the unbiased, 'true', values of the parameters relating trigonometric and photometric parallaxes are:

$$\varpi_g = (1.167 \pm 0.055) \varpi_{bh} - (0.113 \pm 0.039) \text{ mas}. \quad (8)$$

The fact that $k_p > 1$ indicates that the distance scale established by Blaha & Humphreys (1989) must be reduced, $r = k_d r_{bh}$, by the factor $k_d = 1/k_p$ equal to $k_d = 0.86 \pm 0.04$.

Thus, a comparison of trigonometric and photometric parallaxes of OB associations suggests that *Gaia* DR2 parallaxes have a systematic bias of $\Delta\varpi = -0.11 \pm 0.04$ mas and the distance scale established by Blaha & Humphreys (1989) requires a reduction by 10–18%.

3.2 Distance scale to high-luminosity field stars

The catalog of high-luminosity field stars by Blaha & Humphreys (1989) includes 2089 objects with reliable *Gaia* DR2 parallaxes, ϖ_g . Within 2 kpc from the Sun, *Gaia* DR2 trigonometric distances have formally higher precision than the photometric distances of individual stars determined from the color-magnitude calibrations which are accurate to $\sim 0.5^m$ in terms of distance modulus, $m_V - M_V$. The median heliocentric distance of field stars is 1.8 kpc, so we consider them all without selecting objects with the most precise *Gaia* DR2 parallaxes. Figure 2(a) shows the distribution of trigonometric, ϖ_g , and photometric, ϖ_{bh} , parallaxes of young field stars. We can see that distant objects with small parallaxes form a wide cloud of points near the origin. We cannot determine the systematic bias in parallaxes in this case so we just adopt a fixed parallax correction of $\Delta\varpi = -0.113$ mas and introduce it into the equations:

$$\varpi_g - \Delta\varpi = k_p \varpi_{bh}. \quad (9)$$

The parallax correction of $\Delta\varpi = -0.113$ mas was derived for the other part of the catalog of high-luminosity stars, namely for stars located in OB associations. As the distribution of deviations is quite sampled in this case, we use a 4σ criteria instead of 3σ one to exclude the outliers. The least-squares solution of 2038 linear equations with respect to the distance scale coefficient, k_p , gives us its most probable value:

$$\varpi_g - \Delta\varpi = (1.164 \pm 0.010) \varpi_{bh}, \quad (10)$$

which defines the slope of the straight line in Figure 2(a).

The photometric parallaxes of field stars are determined with large and asymmetrically distributed errors, so the calculated value of k_p can be shifted with respect to the true one. We assumed that the distance moduli of field stars are determined with the random error of 0.5^m and estimated the bias in distance scale coefficient k_p using the method described in section 2.1. The systematic shift appears to be:

$$k_p' - k_p^0 = -0.072, \quad (11)$$

so the unbiased value of k_p is $k_p = 1.236$.

The value of $k_p = 1.24.01$ indicates that the distances to young field stars derived by Blaha & Humphreys (1989) must be corrected by a factor $1/k_p = 0.81 \pm 0.01$, i. e. must be shrunk by $19 \pm 1\%$. The root-mean-square deviation of stellar parallaxes from the linear dependence defined by Eq. 10 amounts to 0.5 mas.

Figure 2(b) shows the distribution of the residual values of parallaxes:

$$\varpi_{res} = \varpi_g - k_p \varpi_{bh} - \Delta\varpi \quad (12)$$

We approximated the distribution of residual parallaxes, ϖ_{res} , by a Gauss distribution with the standard deviation of $\sigma = 0.26$ mas, which fits well the observed distribution in the central $\pm 2\sigma$ -interval. It means that the standard deviation of distance moduli of field stars is $\sim 0.5^m$, which is to be expected for distances derived from spectral-luminosity class calibrations in the V-band. However, there are a lot of stars with large residual parallaxes, ϖ_{res} , which show up as broad wings in the distribution and are due to gross errors in both photometric and trigonometric parallaxes.

3.3 Galactic rotation curve

We compared the parameters of the rotation curve derived with the use of trigonometric and photometric

distances to OB associations. Table 2 lists the Galactic coordinates, l and b , as well as trigonometric and photometric distances, r_{ph} and r_g , to 66 OB associations from the catalog by Blaha & Humphreys (1989) including at least 5 stars with known *Gaia* DR2 parallaxes or at least 5 stars with known line-of-sight velocities from the catalog by Barbier-Brossat & Figon (2000). These photometric distances, r_{ph} , are calculated for the short distance scale: $r_{ph} = 0.8 r_{bh}$ (Sitnik & Melnik 1996; Dambis, Melnik & Rastorguev 2001; Melnik & Dambis 2009). Trigonometric distances are determined from *Gaia* DR2 parallaxes: $r_g = 1/\varpi$. Table 2 also presents the median *Gaia* DR2 proper motions of stars of OB associations, μ_l and μ_b , and their uncertainties, $\varepsilon_{\mu l}$ and $\varepsilon_{\mu b}$; median line-of-sight velocities, V_r , and their uncertainties, ε_{vr} ; the number of stars of OB associations with known *Gaia* DR2 parallaxes (and consequently proper motions), n_μ ; the number of stars with known line-of-sight velocity, n_{vr} , from the catalog by Barbier-Brossat & Figon (2000); as well as the total number of stars of the association with known photometry, n_t . The uncertainties $\varepsilon_{\mu l}$, $\varepsilon_{\mu b}$ and ε_{vr} are calculated as half the size of the central interval containing 67% of values of μ_l , μ_b and V_r in the OB association, respectively.

We determined the parameters of the rotation curve and the motion of the Sun towards the apex by solving the set of Bottlinger equations for line-of-light velocities and proper motions of associations:

$$4.74r\mu_l(\cos b)^{-1} = R_0(\Omega - \Omega_0)\cos l - \Omega r\cos b + u_0\sin l - v_0\cos l. \quad (13)$$

$$V_r = R_0(\Omega - \Omega_0)\sin l\cos b \quad (14)$$

$$-u_0\cos l\cos b - v_0\sin l\cos b - w_0\sin b,$$

where the coefficient $4.74 \times r$ transforms proper motions in units mas yr^{-1} into tangential velocities in km s^{-1} ; the factor $(\cos b)^{-1}$ in the left part of Eq. 13 converts local proper motions μ_l measured in the direction parallel to the Galactic plane into the motions in the Galactic plane; Ω and Ω_0 are the angular velocities of the differential circular rotation of the Galactic disk determined at the Galactocentric distances, R , of the center of the association and at the solar distance, R_0 ; the components of the solar motion towards the apex, u_0 , v_0 and w_0 , are directed toward the Galactic center, in the sense of Galactic rotation and toward the Galactic North Pole, respectively.

We expand the difference $\Omega - \Omega_0$ into a power series in $(R - R_0)$:

$$\Omega - \Omega_0 = \Omega'_0(R - R_0) + 0.5\Omega''_0(R - R_0)^2, \quad (15)$$

where Ω'_0 and Ω''_0 are the first and second derivatives taken at the solar distance, R_0 . So the Eqs 13 and 14 can be rewritten in the following way:

$$\begin{aligned} 4.74r\mu_l(\cos b)^{-1} = & -\Omega_0 r\cos b + u_0\sin l - v_0\cos l \\ & + \Omega'_0(R - R_0)(R_0\cos l - r\cos b) \\ & + 0.5\Omega''_0(R - R_0)^2(R_0\cos l - r\cos b), \end{aligned} \quad (16)$$

$$\begin{aligned} V_r = & -u_0\cos l\cos b - v_0\sin l\cos b - w_0\sin b \\ & + \Omega'_0 R_0(R - R_0)\sin l\cos b \\ & + 0.5\Omega''_0 R_0(R - R_0)^2\sin l\cos b, \end{aligned} \quad (17)$$

We solve the sets of equations for proper motions (16) and line-of-sight velocities (17) jointly applying the weight factors, p_{vl} and p_{vr} , which take into account the observational errors, systematic error in proper motions, $\sigma_{\mu s}$, and "cosmic" velocity dispersion:

$$p_{vl} = (\sigma_0^2 + (4.74r\varepsilon_{\mu t})^2)^{-1/2}, \quad (18)$$

$$p_{vr} = (\sigma_0^2 + \varepsilon_{vr}^2)^{-1/2}, \quad (19)$$

where the total error in proper motion μ_l is

$$\varepsilon_{\mu t} = \sqrt{\varepsilon_{\mu l}^2 + \sigma_{\mu s}}, \quad (20)$$

We assume the "cosmic" dispersion to be $\sigma_0 = 7.0 \text{ km s}^{-1}$, which nearly coincide with the root-mean-squared deviation of velocities of OB associations from the Galactic rotation curve (for more details, Dambis, Melnik & Rastorguev 1995, 2001; Melnik & Dambis 2009). The systematic error in *Gaia* DR2 proper motions is supposed to be $\sigma_{\mu s} = 0.055 \text{ mas yr}^{-1}$ (Arenou et al. 2018; Lindegren et al. 2018a; Lindegren et al. 2018b).

Table 2 Distances, proper motions and line-of-sight velocities for OB associations

Association	l deg.	b deg.	r_{ph} kpc	r_g kpc	n_t	μ_l mas yr ⁻¹	μ_b mas yr ⁻¹	n_μ	V_r km s ⁻¹	n_{vr}
SGR OB5	0.04	-1.16	2.42	2.23	30	-1.809±0.226	-0.810±0.120	27	-15.0±13.4	2
SGR OB1	7.54	-0.77	1.26	1.40	65	-1.162±0.062	-1.375±0.123	47	-10.0±2.0	37
SGR OB4	12.11	-0.96	1.92	1.98	15	-1.204±0.103	-1.046±0.139	14	3.5±3.6	9
SER OB1	16.71	0.07	1.53	1.87	43	-1.325±0.098	-0.839±0.098	33	-5.0±4.9	17
SCT OB3	17.30	-0.73	1.33	1.91	10	-2.504±0.166	-0.686±0.114	6	3.3±6.0	8
SER OB2	18.21	1.63	1.60	2.07	18	-2.120±0.156	-0.517±0.082	16	-4.0±5.5	7
SCT OB2	23.17	-0.54	0.80	1.63	13	-2.194±0.327	-0.949±0.093	10	-11.0±8.2	6
VUL OB1	60.30	0.12	1.60	2.03	27	-5.243±0.264	-0.665±0.305	15	5.8±4.6	8
VUL OB4	60.63	-1.22	0.80	2.12	9	-4.620±0.612	-1.392±0.276	6	-2.9±4.3	3
CYG OB3	72.76	2.04	1.83	1.96	40	-7.029±0.138	-0.737±0.085	32	-10.0±1.8	29
CYG OB1	75.84	1.12	1.46	1.78	71	-6.213±0.115	-0.638±0.066	62	-13.5±1.5	34
CYG OB9	77.81	1.80	0.96	1.68	32	-5.977±0.161	-0.650±0.157	22	-19.5±2.8	10
CYG OB8	77.92	3.36	1.83	1.78	21	-6.034±0.122	0.479±0.245	20	-21.0±3.7	9
CYG OB2	80.27	0.88	1.46	1.62	15	-4.845±0.128	-0.359±0.027	9		0
CYG OB7	88.98	0.03	0.63	0.91	29	-2.030±0.780	-0.961±0.159	22	-9.4±2.0	21
CEP OB2	102.02	4.69	0.73	0.97	56	-3.663±0.228	-0.580±0.204	45	-17.0±1.1	36
CEP OB1	104.20	-0.94	2.78	4.32	58	-4.426±0.114	-0.608±0.058	44	-58.2±1.8	17
CEP OB5	108.50	-2.69	1.67	3.43	6	-3.392±0.210	-0.969±0.210	6	-48.7±20.6	2
CAS OB2	111.99	-0.00	2.10	3.42	41	-3.923±0.144	-0.642±0.119	30	-50.1±4.2	7
CEP OB3	110.71	3.13	0.70	0.85	25	-1.891±0.171	-1.115±0.143	18	-22.9±0.9	18
CAS OB5	116.09	-0.50	2.01	3.46	52	-3.471±0.058	-0.941±0.058	45	-45.8±1.8	16
CEP OB4	118.21	5.25	0.66	1.06	7	-1.957±0.029	-1.144±0.154	7	-24.0	1
CAS OB4	120.05	-0.30	2.30	2.84	27	-2.923±0.147	-0.535±0.099	24	-37.0±3.3	7
CAS OB14	120.36	0.74	0.88	1.51	8	-1.630±0.384	-0.882±0.266	6	-15.0±3.5	4
CAS OB7	122.98	1.22	2.01	3.10	39	-2.328±0.067	-0.387±0.044	35	-50.0±0.5	4
CAS OB1	124.73	-1.73	2.01	2.31	11	-1.345±0.257	-1.076±0.137	7	-42.0±1.1	5
CAS OB8	129.16	-1.06	2.30	3.15	43	-0.996±0.025	-0.498±0.031	41	-34.6±2.6	14
PER OB1	134.70	-3.14	1.83	2.59	163	-0.120±0.035	-1.188±0.029	150	-43.2±0.8	80
CAS OB6	134.95	0.72	1.75	2.36	45	-0.241±0.104	-0.723±0.132	29	-42.6±2.3	12
CAM OB1	141.08	0.89	0.80	1.22	50	0.232±0.135	-1.118±0.122	41	-11.0±1.7	30
CAM OB3	146.97	2.85	2.65	5.48	8	-0.032±0.029	0.127±0.104	6	-27.6±11.1	3
PER OB2	160.22	-16.55	0.32	0.41	7	4.905±0.448	-0.633±0.684	5	21.2±1.7	7
AUR OB1	173.83	0.14	1.06	1.80	36	2.621±0.144	-1.806±0.109	31	-1.9±2.7	26
ORI OB1	206.90	-17.71	0.40	0.39	68	0.928±0.212	0.633±0.126	54	25.4±1.0	62

Table 2 continued

Association	l deg.	b deg.	r_{ph} kpc	r_g kpc	n_t	μ_l mas yr ⁻¹	μ_b mas yr ⁻¹	n_μ	V_r km s ⁻¹	n_{vr}
AUR OB2	173.33	-0.16	2.42	3.24	20	1.928±0.173	-1.188±0.072	16	-2.6±2.5	4
NGC 1893	173.60	-1.70	2.90	3.36	10	1.035±0.176	-1.284±0.062	6		0
GEM OB1	188.96	2.22	1.21	2.26	40	1.900±0.113	-0.713±0.076	35	16.0±1.2	18
MON OB1	202.08	1.08	0.58	0.87	7	1.348±0.347	-2.315±0.419	6	23.4±4.9	7
MON OB2	207.35	-1.60	1.21	1.60	31	-0.782±0.119	-1.663±0.146	23	23.0±2.3	25
CMA OB1	224.58	-1.56	1.06	1.30	17	-2.781±0.224	-2.861±0.280	16	34.3±5.7	8
COLL 121	238.42	-8.41	0.55	0.65	13	-5.626±0.281	-1.192±0.227	8	29.6±2.2	10
NGC 2362	237.82	-5.96	1.21	1.46	8	-4.024±0.540	-0.964±0.153	3	18.0±6.3	5
NGC 2439	245.27	-4.08	3.50	4.12	23	-3.910±0.077	-0.579±0.041	22	62.7	1
PUP OB1	243.53	0.16	2.01	4.22	22	-3.791±0.065	-0.857±0.061	16	77.0	1
PUP OB2	244.61	0.58	3.18	5.74	13	-3.440±0.345	-0.652±0.228	9		0
COLL 140	244.42	-7.33	0.29	0.42	6	-6.974±0.287	-4.512±0.598	6	10.3±3.0	5
VELA OB2	262.05	-8.52	0.40	0.40	13	-9.620±0.605	-0.127±0.380	9	24.0±2.7	13
VELA OB1	264.83	-1.41	1.46	2.06	46	-6.978±0.092	-1.461±0.078	43	23.0±1.0	18
CAR OB1	286.45	-0.46	2.01	2.99	126	-7.581±0.079	-0.731±0.033	101	-5.0±1.3	39
TR 16	287.25	-0.25	2.10	2.72	18	-7.300±0.099	-1.067±0.077	14	-1.0±1.5	5
COLL 228	287.57	-0.98	2.01	3.10	15	-6.556±0.105	-1.538±0.065	13	-13.0±3.0	9
CAR OB2	290.39	0.12	1.83	3.10	59	-6.467±0.064	-1.152±0.044	48	-8.2±1.8	22
CRU OB1	294.87	-1.06	2.01	2.82	75	-6.161±0.054	-1.034±0.033	65	-5.3±1.5	33
NGC 3766	294.12	-0.02	1.53	2.40	11	-6.649±0.028	-1.038±0.031	10	-15.6±0.5	2
CEN OB1	304.14	1.44	1.92	2.27	103	-4.712±0.061	-1.090±0.034	85	-19.0±2.6	32
NGC 5606	314.87	0.99	1.53	2.50	5	-5.622±0.040	-0.862±0.059	5	-37.8±1.0	3
PIS 20	320.39	-1.48	3.18	3.38	6	-4.845±0.095	-0.694±0.097	5	-49.0	1
NOR OB1	328.05	-0.92	2.78	2.52	8	-3.946±0.094	-0.699±0.110	7	-35.6±2.7	6
NGC 6067	329.71	-2.18	1.67	2.03	9	-3.250±0.071	-0.454±0.075	8	-40.0±0.9	8
R 103	332.36	-0.74	3.18	2.93	33	-3.843±0.273	-0.827±0.086	26	-47.5±8.2	10
ARA OB1B	337.95	-0.85	2.78	2.47	21	-2.511±0.092	-0.936±0.081	19	-34.7±3.4	9
ARA OB1A	337.68	-0.92	1.10	1.16	53	-2.064±0.137	-2.629±0.231	42	-36.3±7.3	8
NGC 6204	338.34	-1.16	2.20	2.83	13	-2.079±0.038	-0.598±0.062	5	-51.0±2.6	5
SCO OB1	343.72	1.37	1.53	1.67	73	-1.823±0.038	-0.806±0.041	66	-28.8±2.9	28
SCO OB2	351.29	19.02	0.13	0.15	10	-23.339±0.791	-8.307±0.132	4	-4.1±0.7	10
SCO OB4	352.64	3.23	0.96	1.20	11	-0.633±0.189	-2.672±0.083	10	3.0±2.4	7

We adopted a solar Galactocentric distance to be of $R_0 = 7.5$ kpc (Glushkova et al. 1998; Nikiforov 2004; Feast et al. 2008; Groenewegen, Udalski & Bono 2008; Reid et al. 2009; Dambis et al. 2013; Francis & Anderson 2014; Boehle et al. 2016; Branham 2017).

Table 3 lists the parameters of the Galactic rotation curve, Ω_0 , Ω'_0 and Ω''_0 , and the solar motion towards the apex, u_0 and v_0 , calculated for two sets of distances to OB associations: photometric and trigonometric ones. We use the median proper motions and line-of-sight velocities derived from kinematical data of at least 5 member stars, $n_\mu \geq 5$ or $n_{vr} \geq 5$, respectively. Given that Gaia DR2 proper motions and line-of-sight velocities from the catalog by Barbier-Brossat & Figon (2000) are available for 90% and 52% of OB association stars, respectively, adopting the minimal number of stars with the corresponding data equal to 5, $n_\mu \geq 5$ or $n_{vr} \geq 5$, gives us noticeably different numbers of conditional equations for proper motions and line-of-sight velocities: 64 and 50, respectively. Table 3 also lists the value of the Oort constant, $A = -0.5\Omega'_0 R_0$, and the standard deviation of the velocities from the rotation curve, σ_0 . It also gives the number of conditional equations for proper motions (Eq. 16) and line-of-sight velocities (Eq. 17) in the form: $N_\mu + N_{vr}$. OB associations and young field stars are located close to the Galactic plane and the component of the solar velocity, w_0 , is poorly determined from the solution of equations for line-of-sight velocities, and we therefore adopted the value of $w_0 = 7.0$ km s⁻¹.

We simulated the distribution of random errors in distance moduli, DM , and in trigonometric parallaxes, ϖ_g , to estimate the biases in the parameters of the rotation curve and the solar motion towards the apex. The distribution of true distances is supposed to be close to the observed distances. We calculated the true values of the proper motions μ_l (Eq. 16) and velocities V_r (Eq. 17) using observational distances and the parameters listed in Table 3 and added to them normally distributed errors with the standard deviations $\varepsilon_{\mu l}$ and ε_{vr} , respectively. We then simulated "wrong" distances and solved the systems of Eqs 16 and 17 to determine the parameters of the rotation curve and the solar motion. We repeated this procedure 10^3 times. The average shifts between the calculated and true values of the parameters are also listed in Table 3. We can see that the systematic corrections to the parameters obtained for the sample of OB associations do not exceed $\sim 10\%$ of the values of random errors. Such small values of systematic errors are due to the great accuracy of the relative distances (without consideration of the distance-scale uncertainty) to OB associations.

It follows from Table 3 that the values of the parameters of the Galactic rotation curve and the solar motion towards the apex, Ω_0 , Ω'_0 , Ω''_0 , u_0 and v_0 , derived with photometric and trigonometric distances to OB associations are consistent within the errors. The angular velocity of the Galactic disk at the solar distance, Ω_0 , calculated for the two distance scales has the same values of 30.0 ± 0.70 km s⁻¹ kpc⁻¹. Such a good agreement is due to the fact that both the left-hand part of Eq. 16 ($4.74r\mu_l \cos b^{-1}$) and the term with Ω_0 in the right-hand part ($-\Omega_0 r \cos b$) are proportional to the distance r , and hence distance-scale changes have little effect on the inferred angular velocity Ω_0 . Note that Bobylev & Bajkova (2019) obtained a similar value of Ω_0 equal to $\Omega_0 = 29.7 \pm 0.1$ km s⁻¹ kpc⁻¹ from an analysis of the *Gaia* DR2 data for a sample of OB stars.

We also derived the parameters of the rotation curve and the solar motion from the kinematics of high luminosity field stars. The parameters Ω_0 , Ω'_0 , Ω''_0 , u_0 and v_0 were also calculated for two sets of distances (Table 3). Here the weight factors (Eqs 18 and 19) were computed with the use of the uncertainties $\varepsilon_{\mu l}$ and ε_{vr} of measurements of proper motions and line-of-sight velocities of individual stars. We excluded from consideration the velocities of objects deviating more than 40 km s⁻¹ from the rotation curve, so the numbers of conditional equations ($N_\mu + N_{vr}$) are a bit different for photometric (1899+913) and trigonometric (1915+911) sets of distances.

Table 3 also lists the systematic errors and corrected parameters of the rotation curve and the solar motion calculated for the sample of field stars. Here the systematic errors appear to be comparable to the random errors, so we corrected the calculated values of the parameters for the systematic shift.

We can see that the parameters derived for two sets of distances to field stars agree within the errors. Moreover, the parameters obtained for OB associations and field stars are consistent within the errors.

Figure 3 shows two rotation curves of the Galaxy and the azimuthal velocities of OB associations calculated for photometric and trigonometric distances to OB associations. The corresponding values of the rotation velocity at the solar distance are $\Theta_0 = 225$ and 222 km s⁻¹, respectively. We can see that the two rotation curves are practically flat in the 3-kpc solar neighborhood. On the whole, the differences in the two rotation curves can be thought to be insignificant.

We also calculated the parameters of the rotation curve and the solar motion towards the apex for the solar Galactocentric distance $R_0 = 8.2$ kpc (Gravity Collaboration et al. 2019). For the set of photometric distances to OB associations, we obtained the

Table 3 Parameters of the Galactic rotation curve and the solar motion towards the apex

Objects	Ω_0	Ω'_0	Ω''_0	u_0	v_0	A	σ_0	$N_\mu + N_{vr}$
Distance scale	km s ⁻¹ kpc ⁻¹	km s ⁻¹ kpc ⁻²	km s ⁻¹ kpc ⁻³	km s ⁻¹	km s ⁻¹	km s ⁻¹ kpc ⁻¹	km s ⁻¹	
OB associations	30.03	-4.56	1.04	6.53	11.46	17.10	6.8499	64+50
$r_{ph} = 0.8 r_{bh}$	± 0.73	± 0.16	± 0.14	± 0.95	± 1.22	± 0.60		
systematic errors	-0.05	0.01	-0.01	-0.01	-0.05	-0.03		
OB associations	29.57	-4.20	0.72	8.52	8.57	15.75	7.5792	64+50
$r_{tg} = 1/\varpi_g$	± 0.62	± 0.15	± 0.14	± 1.06	± 1.24	± 0.56		
systematic errors	-0.02	0.01	-0.01	-0.01	-0.06	-0.03		
Field stars	28.70	-4.20	0.88	6.72	9.78	15.75	13.0948	1899+913
$r_{ph} = 0.8 r_{bh}$	± 0.20	± 0.06	± 0.03	± 0.36	± 0.41	± 0.23		
systematic errors	0.01	0.08	-0.11	0.14	-0.87	-0.30		
corrected values	28.69	-4.28	0.99	6.58	10.65	16.05		
Field stars	28.68	-4.20	0.88	7.43	9.56	15.75	13.1919	1915+911
$r_{tg} = 1/\varpi_g$	± 0.18	± 0.05	± 0.02	± 0.36	± 0.40	± 0.19		
systematic errors	-0.20	0.17	-0.13	0.33	-0.97	-0.64		
corrected values	28.88	-4.37	1.01	7.10	10.53	16.39		

following values: $\Omega_0 = 30.09 \pm 0.73$ km s⁻¹ kpc⁻¹, $\Omega'_0 = -4.13 \pm 0.15$ km s⁻¹ kpc⁻², $\Omega''_0 = 0.85 \pm 0.12$ km s⁻¹ kpc⁻³, $u_0 = 6.75 \pm 0.94$ km s⁻¹, $v_0 = 11.86 \pm 1.21$ km s⁻¹ and $A = 16.95 \pm 0.62$ km s⁻¹ kpc⁻¹, which all except Ω'_0 agree well with those computed for $R_0 = 7.5$ kpc (first row of Table 3). We can see that the value of Ω'_0 decreases with increasing R_0 , but the value of the Oort constant $A = -0.5\Omega'_0 R_0$ remains nearly the same. The rotation curve obtained for $R_0 = 8.2$ kpc is also nearly flat, but the value of Θ_0 amounts to 247 km s⁻¹ here.

Here we supposed that the centroid of OB associations rotates with the velocity, v_φ , which is nearly equal to the velocity of the rotation curve, v_c . The difference between them, $v_\varphi - v_c$, the so-called asymmetric drift, is determined by the Jeans equation and can be estimated from the following formula:

$$v_\varphi - v_c = \frac{\overline{\sigma_R^2}}{80} \text{ km s}^{-1}, \quad (21)$$

where σ_R is the radial velocity dispersion of the disk subsystem considered (Binney & Tremaine 2008). For the sample of OB associations, we adopted the value of $\sigma_R = 9$ km s⁻¹ and found the asymmetric drift to be $v_\varphi - v_c \approx 1$ km s⁻¹, which corresponds to the uncertainty of 0.1 km s⁻¹ kpc⁻¹ in the value of Ω_0 , what amounts to only 18% of its random error (Table 3).

So the centroid of OB associations can be thought to rotate with the velocity of the rotation curve.

Table 3 shows that the solar azimuthal velocity determined with respect to the centroid of OB associations, v_0 , lies in the range 8–12 km s⁻¹ which is consistent with the values obtained in other studies (Schonrich, Binney, Dehnen 2010; Tian et al. 2015; Bobylev & Bajkova 2018).

3.4 Residual velocities of OB associations in the Galactic plane

Residual velocities are the observed heliocentric velocities corrected for the Galactic rotation and the solar motion towards the apex: $V_{res} = V_{obs} - V_{rot} - V_{ap}$. The residual velocities show how well objects follow the Galactic rotation law and are indicators of non-circular motions. In this section we consider residual velocities in the Galactic plane directed in the radial and azimuthal directions. The radial component of the residual velocity, V_R , is directed along the Galactic radius-vector and its positive value corresponds to the motion away from the Galactic center while the azimuthal component, V_T , is tangent to circular orbits and its positive value corresponds to an additional velocity in the sense of Galactic rotation. Note that residual velocities are nearly independent on the choice of the solar Galactocentric distance in the range 7–9 kpc.

Figure 4 shows the distribution of the residual velocities of OB associations in the Galactic plane calculated with photometric and trigonometric distances. The residual velocities computed with the photometric distance scale are determined with respect to the rotation curve calculated with photometric distances and vice versa (Table 3). Figure 4 shows only OB associations with the median velocities derived from at least 10 proper motions ($n_\mu \geq 10$) and 5 line-of-sight velocities ($n_{vr} \geq 5$) of member stars. The root-mean-square differences, ΔV_R and ΔV_T , between residual velocities calculated with trigonometric and photometric distances amount to $\Delta V_R = 3.6$ and $\Delta V_T = 5.8$ km s⁻¹, respectively. The residual velocities of the Per OB1 and Cep OB1 associations appear to be the most sensitive to the choice of the distance scale. The radial residual velocity, V_R , of the Per OB1 association changes by 8 km s⁻¹: from $V_R = -6.6$ km s⁻¹ ($r_{ph} = 1.83$ kpc) to 1.7 km s⁻¹ ($r_{tg} = 2.58$ kpc), which corresponds to the greatest change in the velocity V_R among OB associations considered. The Cep OB1 association demonstrates the greatest change in the azimuthal residual velocity V_T : from $V_T = -11.6$ km s⁻¹ ($r_{ph} = 2.78$ kpc) to +8.9 km s⁻¹ ($r_{tg} = 4.32$ kpc), i.e. by 21 km s⁻¹.

Figure 4 also shows the boundaries of the Sagittarius, Scorpio, Carina, Cygnus, Local System and Perseus star-gas complexes identified by Efremov & Sitnik (1988). A comparison of the residual velocities calculated for the two distance scales suggests that the greatest changes take place in the Perseus complex. In the photometric distance scale the majority of OB associations in the Perseus complex have the radial velocity V_R directed towards the Galactic center while in the trigonometric distance scale their velocities V_R are close to zero. Note that the direction of the radial residual velocities in the Perseus complex is the foundation for all models of the Galactic spiral structure and the Galactic resonance rings (see section 4).

Figure 5 illustrates the appearance of systematic stream motions due to the choice of a wrong distance scale. We scattered test particles randomly over the galactic disk within 3.5 kpc from the solar position and assigned to them the velocities corresponding to the Galactic rotation law which means that the residual velocities equal zero (Fig. 5a). For simplicity we adopted the flat rotation curve with the angular velocity at the solar distance equal to $\Omega_0 = 30$ km s⁻¹ kpc⁻¹. Let us suppose that we do not know the true distances, corresponding to the short distance scale ($r_{ph} = 0.8 r_{bh}$) but use instead of them the distances corresponding to the long distance scale established by *Gaia* DR2 parallaxes: $r_{tg} = (1.17/r_{bh} - 0.11)^{-1}$ (Eq. 8). Figure 5(b) shows how the wrong distance scale affects the residual velocities. The use of the trigonometric distance scale causes

the appearance of spurious residual velocities which are absent in the photometric distance scale.

Figure 5 shows that the spurious residual velocities are very small in the vicinity of 1 kpc from the Sun ($|V_R| < 3$ and $|V_T| < 3$ km s⁻¹). However, objects located at distances 2–3 kpc from the Sun demonstrate significant (10–20 km s⁻¹) spurious residual velocities. In quadrant II, where the Perseus complex is located, the spurious systematic motions are directed away from the Galactic center and in the sense of Galactic rotation. Generally, the radial component, V_R , of the spurious residual velocities is directed towards the Galactic center in quadrants III and IV and away from it in quadrants I and II, whereas the azimuthal component, V_T , is directed in the sense of Galactic rotation in quadrants II and III and in the opposite sense in quadrants I and IV. Note that the detection of a similar picture in the distribution of residual velocities can suggest a need to shrink the distance scale.

3.5 Motion in the Z-direction

The residual velocities of OB associations in the direction perpendicular to the Galactic plane, V_z , are determined with the use of both proper motions along Galactic latitude, μ_b , and line-of-sight velocities, V_r :

$$V_z = 4.74\mu_b r \cos b + V_r \sin b + w_0, \quad (22)$$

where w_0 is the velocity of the Sun in the Z-direction.

Eq. (22) indicates that the first term ($4.74\mu_b r \cos b$) depends on the distance r , and hence the uncertainties in distances can create spurious motions in Z-direction. Two conditions must be fulfilled for their appearance: objects must not lie precisely in the Galactic plane ($b \neq 0$) and the distance scale must be wrong.

If objects are distributed symmetrically with respect to the Galactic plane then a wrong distance scale does not give rise to systematic motions: objects lying above and below the Galactic plane must acquire the additional velocities V_z in opposite directions which causes only an increase in the velocity dispersion.

However, the gas disk in the Galaxy is rippled and young stars born in it often lie 50–100 pc above or below the Galactic plane. For example, all associations in the Cygnus complex (Cyg OB1, Cyg OB3, Cyg OB8, Cyg OB9) are located above the Galactic plane ($b = +1..+3^\circ$) (see Table 2), which corresponds to the shift of $\Delta z = 50$ –130 pc above the plane. Here we adopted the position of the Sun with respect to the Galactic plane to be $z_0 = 20$ pc. On the contrary, the Per OB1 association is located below the Galactic plane ($b =$

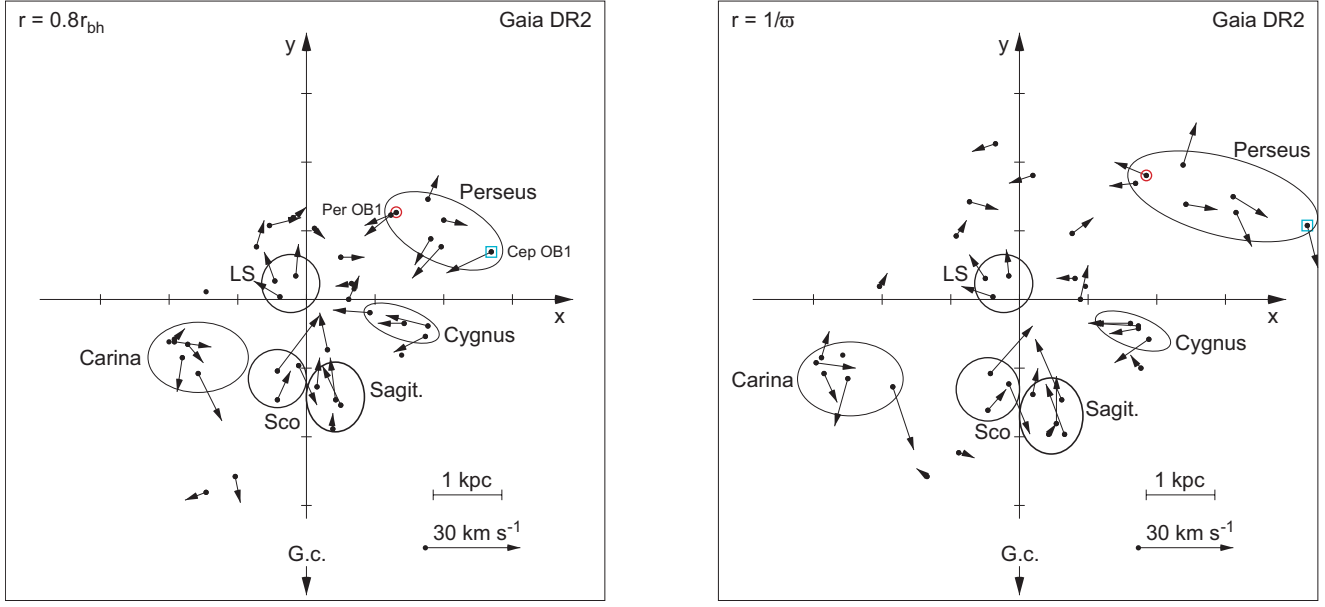


Fig. 4 Distribution of the residual velocities of OB associations calculated with photometric and trigonometric distances. We present only associations with $n_{vr} \geq 5$ and $n_\mu \geq 10$. Associations with small residual velocities ($|V_R| < 3$ and $|V_T| < 3$ km s⁻¹) are shown by black circles without any vector. The Per OB1 association (marked by the red circle) and the Cep OB1 association (marked by the blue square) have the residual velocities V_R (Per OB1) and V_T (Cep OB1) depending most strongly on the choice of the distance scale. Also show are the boundaries of the Sagittarius, Scorpius, Carina, Cygnus, Local System and Perseus star-gas complexes. The x -axis is directed in the sense of Galactic rotation and the y -axis points away from the Galactic center. The Sun is at the origin. The Galactic center (G. c.) is in the bottom.

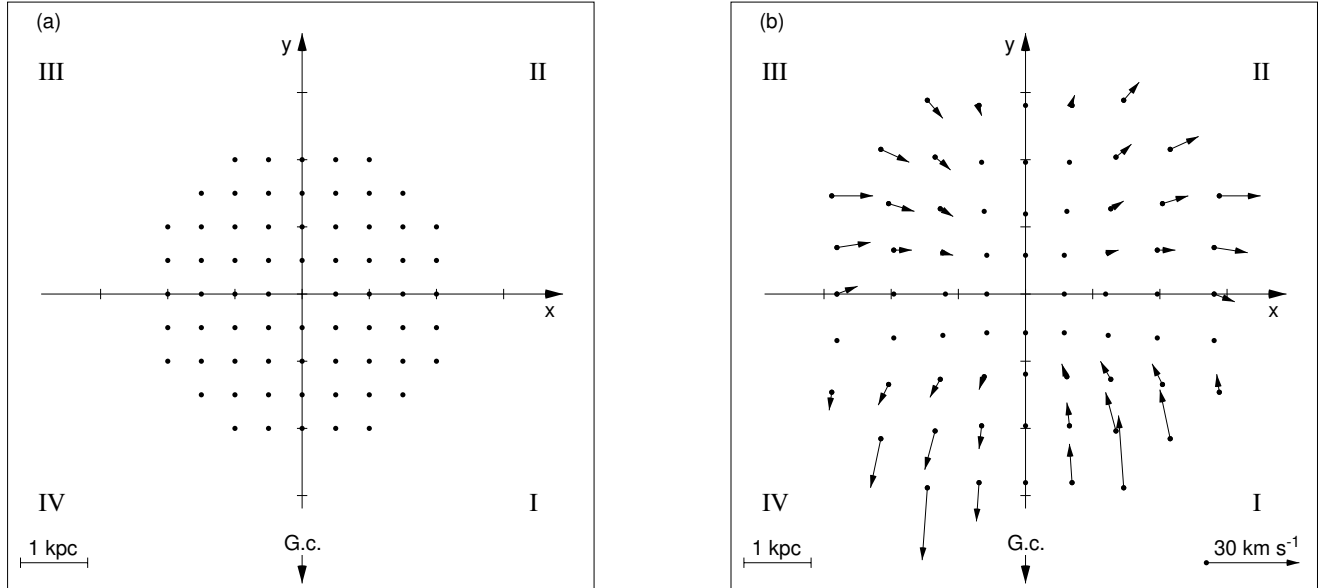


Fig. 5 Spurious systematic motions emerging from the choice of the wrong distance scale. (a) The initial distribution of the residual velocities of test particles determined in the short distance scale of OB associations ($r_{ph} = 0.8 r_{bh}$). (b) The residual velocities calculated with the use of the trigonometric distance scale, $r_{tg} = (1.17/r_{bh} - 0.11)^{-1}$. Roman numerals indicate the quadrants. The radial component, V_R , of the spurious residual velocities is directed towards the Galactic center in quadrants III and IV and away from it in quadrants I and II while the azimuthal component, V_T , is directed in the sense of galactic rotation in quadrants II and III and in the opposite sense in quadrants I and IV. Particles with small residual velocities ($|V_R| < 3$ and $|V_T| < 3$ km s⁻¹) are shown by black circles without any vector. The x -axis is directed in the sense of Galactic rotation and the y -axis points away from the Galactic center. The Sun is at the origin. The Galactic center is in the bottom.

-3.14°) being shifted at $\Delta z = -80$ pc with respect to the plane.

A ripple on the Galactic gas disk and a wrong distance scale can give rise to spurious systematic motions in the direction perpendicular to the Galactic plane. The root-mean-square difference between the velocities V_z calculated with photometric and trigonometric distances is 2.1 km s^{-1} . To illustrate the emergence of spurious systematic motions in the Z -direction we list the residual velocities V_z for several OB associations determined for the two distance scales. Table 4 presents the Galactic coordinates, distances and residual velocities V_z obtained for the Per OB1, Cyg OB3, Cep OB1 and Cep OB2 associations located above or below the Galactic plane. We can see that the velocities V_z derived for the photometric and trigonometric distance scales differ, on average, by 2 km s^{-1} but the danger is that this effect is systematic.

We solved the system of equations (22) with respect to the solar velocity in the Z -direction, w_0 , for 50 OB associations with median velocities derived from at least 5 proper motions ($n_\mu \geq 5$) and 5 line-of-sight velocities ($n_{vr} \geq 5$) of member stars to obtain the values of $w_0 = 7.15 \pm 0.45$ and $9.26 \pm 0.63 \text{ km s}^{-1}$ for the photometric and trigonometric distance scale, respectively. The corresponding velocity dispersions in the vertical direction, σ_z , calculated for the two distance scales have values of $\sigma_z = 3.4$ and 4.4 km s^{-1} .

Note that the analysis of the kinematics of high-luminosity field stars yields very similar values of the solar vertical velocity: $w_0 = 7.34 \pm 0.31 \text{ km s}^{-1}$ (887 equations) and $8.43 \pm 0.32 \text{ km s}^{-1}$ (902 equations) obtained for photometric and trigonometric distance scales, respectively. We excluded field stars with the residual velocities, V_z , greater than 40 km s^{-1} . The vertical velocity dispersions of field stars derived for the two distance scales are $\sigma_z = 8.9$ and 9.2 km s^{-1} , respectively.

4 Discussion and conclusions

We calculated the median parallaxes for 47 OB associations including at least 10 member stars with known *Gaia* DR2 parallaxes. The comparison of trigonometric and photometric parallaxes to OB associations revealed the zero-point displacement of *Gaia* DR2 parallaxes equal to $\Delta\varpi = -0.11 \pm 0.04 \text{ mas}$, which means that *Gaia* DR2 parallaxes are, on average, underestimated and distances derived from them must be reduced.

Arenou et al. (2018, Table 1 there) compared *Gaia* DR2 parallaxes with parallaxes of $\sim 6 \times 10^4$ stars measured by the Hipparcos satellite. The average visual

magnitude and the zero-point offset of stars in their sample are $\overline{G} = 8.3^m$ and $\Delta\varpi = -0.118 \pm 0.003 \text{ mas}$, respectively. The average visual magnitude of stars of OB associations cross-matched with *Gaia* DR2 is $\overline{G} = 8.5^m$ and our value of the zero-point correction, $\Delta\varpi = -0.11 \pm 0.04$, agrees with the estimate by Arenou et al. (2018).

Furthermore, the analysis of parallaxes of OB associations and high-luminosity stars in field confirmed our previous conclusion (Dambis, Melnik & Rastorguev 2001; Melnik & Dambis 2009) that the distance scale to OB associations established by Blaha & Humphreys (1989) must be reduced by 10–20%.

We investigated how the choice of a wrong distance scale influences the parameters of the rotation curve and found that the parameters calculated with the use of photometric and trigonometric distances are consistent within the errors. In particular, the angular velocity of the Galactic disk at the distance of the Sun, Ω_0 , computed with the use of photometric and trigonometric distances to OB associations has the values of 30.0 ± 0.7 and $29.6 \pm 0.6 \text{ km s}^{-1} \text{ kpc}^{-1}$, respectively (Table 3).

The analysis of the residual velocities of OB associations (i.e. velocities corrected for the Galactic rotation and the solar motion towards the apex) shows that they depend strongly on the choice of the distance scale. The root-mean-square differences between the residual velocities calculated with the use of photometric and trigonometric distances in projection on the Galactic radius vector, azimuthal and vertical directions are $\Delta V_R = 3.6$, $\Delta V_T = 5.8$ and $\Delta V_z = 2.1 \text{ km s}^{-1}$, respectively. A wrong distance scale can give rise to spurious systematic motions. The distance scale determined by *Gaia* DR2 parallaxes creates systematic motions with the radial component, V_R , directed towards the Galactic center in quadrants III and IV and away from it in quadrants I and II and with the azimuthal component, V_T , directed in the sense of Galactic rotation in quadrants II and III and in the opposite sense in quadrants I and IV. A discovery of a similar velocity distribution can suggest the need to reduce the distance scale.

The residual velocities of objects located in the Perseus star-gas complex appeared to be most sensitive to the choice of the distance scale. In the case of the short photometric distance scale ($r_{ph} = 0.8 r_{bh}$) young stars of the Perseus complex demonstrate conspicuous systematic motions in the direction toward the Galactic center ($V_R = -6.7 \pm 2.7 \text{ km s}^{-1}$), whereas in the case of the trigonometric (uncorrected) distance scale these motions vanish ($V_R = -0.9 \pm 3.0$) being balanced by spurious systematic motions.

Table 4 Residual velocities V_z of some OB associations

name	l deg	b deg	r_{ph} kpc	r_{tg} kpc	Δz kpc	$V_z(r_{ph})$ km s ⁻¹	$V_z(r_{tg})$ km s ⁻¹
Cyg OB3	72.76	2.04	1.83	1.95	0.085	0.3	2.0
Cep OB2	102.01	4.69	0.73	0.99	0.080	3.4	4.9
Cep OB1	104.20	-0.94	2.78	4.32	-0.026	0.0	-2.4
Per OB1	134.70	-3.14	1.83	2.58	-0.080	-0.9	-3.1

The position of the density-wave spiral arms (Lin & Shu 1964) inside the corotation circle (the radius at which the spiral pattern rotates at the angular velocity equal to the angular velocity of the Galactic disk) corresponds to the radial velocity component directed toward the Galactic center ($V_R < 0$). Lin et al. (1969) suggest that the Galactic spiral pattern rotates with the angular velocity of $\Omega_s = 13$ km s⁻¹ kpc⁻¹, which puts the Perseus complex inside the corotation circle, $\Omega_s < \Omega(R_{per})$. It is just the velocities directed toward the Galactic center in the Perseus complex that are the foundation for the concept of the Galactic spiral structure and its modification for the four-armed spiral pattern (Burton & Bania 1974; Georgelin & Georgelin 1976; Russeil 2003; Rastorguev et al. 2017; Bobylev & Bajkova 2018; Vallée 2019).

Another model of the Galaxy includes the bar and a two-component outer ring $R_1 R_2$ rotating with the angular velocity of the bar $\Omega_b \approx 50$ km s⁻¹ kpc⁻¹. Here also the direction of the residual velocities V_R in the Perseus complex is of great importance: their direction toward the Galactic center suggests the location of the Perseus region in the outer resonance ring R_2 (Melnik & Rautiainen 2009, 2011; Rautiainen & Melnik 2010; Melnik et al. 2015, 2016; Melnik 2019).

5 Acknowledgements

We thank the anonymous referee and the Editor for useful remarks and suggestions. This work has made use of data from the European Space Agency (ESA) mission *Gaia* (<https://www.cosmos.esa.int/gaia>), processed by the *Gaia* Data Processing and Analysis Consortium (DPAC, <https://www.cosmos.esa.int/web/gaia/dpac/consortium>). Funding for the DPAC has been provided by national institutions, in particular the institutions participating in the *Gaia* Multilateral Agreement. This

research has made use of the Vizier catalogue access tool, CDS, Strasbourg, France. The original description of the Vizier service was published by Ochsenbein, Bauer & Marcout (2000). A. K. acknowledges the support from the Russian Foundation for Basic Research (project nos. 18-02-00890 and 19-02-00611).

References

- Ambartsumian, V. A.: 1949, *Soviet Astron.*, 26, 3
- Arenou, F., Luri, X., Babusiaux, C., et al.: 2018, *Astron. Astrophys.*, 616, 17
- Barbier-Brossat, M., Figon, P.: 2000, *Astron. Astrophys. Suppl. Ser.*, 142, 217
- Blaauw A., 1964, *ARA&A*, 2, 213
- Berdnikov, L.N., Dambis, A.K., Vozyakova, O.V.: 2000, *Astron. Astrophys. Suppl. Ser.*, 143, 211
- Binney J., Tremaine S., *Galactic Dynamics*, Second Edition. Princeton Univ. Press, Princeton, New Jersey, 2008.
- Blaha, C., Humphreys, R. M.: 1989, *Astron. J.*, 98, 1598
- Bobylev, V. V., Bajkova, A. T.: 2018, *Astron. Lett.* 44, 676
- Bobylev, V. V., Bajkova, A. T.: 2019, *Astron. Lett.* 45, 331
- Boehle, A., Ghez, A. M., Schödel, R. et al.: 2016, *Astrophys. J.*, 830, 17
- Branham, R. L.: 2017, *Astrophys. Space Sci.*, 362, 29
- Bressan, A., Marigo, P., Girardi, L., Salasnich, B., Dal Cero, C., Rubele, S., Nanni, A.: 2012, *Mon. Not. R. Astron. Soc.*, 427, 127
- Burton, W. B., Bania, T. M.: 1974, *Astron. Astrophys.*, 33, 425
- Carrillo, I., Minchev, I., Steinmetz, M., et al.: 2019, *Mon. Not. R. Astron. Soc.*, 490, 797
- Dambis, A. K., Berdnikov, L. N., Kniazev, A. Y. et al.: 2013, *Mon. Not. R. Astron. Soc.*, 435, 3206
- Dambis, A. K., Melnik, A. M., Rastorguev, A. S.: 1995, *Astron. Lett.* 21, 291
- Dambis, A. K., Melnik, A. M., Rastorguev, A. S.: 2001, *Astron. Lett.*, 27, 58
- Efremov Yu. N., Sitnik T. G.: 1988, *Soviet Astron. Lett.* 14, 347
- ESA 1997, The HIPPARCOS and TYCHO catalogues. Astrometric and photometric star catalogues derived from the ESA HIPPARCOS Space Astrometry Mission, ESA SP, 1200
- Feast, M. W., Laney, C. D., Kinman, T. D., van Leeuwen, F., Whitelock, P. A.: 2008, *Mon. Not. R. Astron. Soc.*, 386, 2115
- Fragkoudi, F., Katz, D., Trick, W., et al.: 2019, *Mon. Not. R. Astron. Soc.*, 488, 3324
- Francis, Ch., Anderson, E.: 2014, *Mon. Not. R. Astron. Soc.*, 441, 1105
- Gaia Collaboration, Brown, A. G. A., Vallenari, A., et al.: 2018a, *Astron. Astrophys.*, 616, A1
- Gaia Collaboration, Katz, D., Antoja, T., et al.: 2018b, *Astron. Astrophys.*, 616, A11
- Gaia Collaboration, Prusti, T., de Bruijne, J. H. J., et al.: 2016, *Astron. Astrophys.*, 595, A1
- Georgelin, Y. M., Georgelin, Y. P.: 1976, *Astron. Astrophys.*, 49, 57
- Glushkova, E. V., Dambis, A. K., Melnik, A. M., Rastorguev, A. S.: 1998, *Astron. Astrophys.*, 329, 514
- Gravity Collaboration, Abuter, R., Amorim, A., et al.: 2019, *Astron. Astrophys.*, 625, 10
- Groenewegen, M. A. T., Udalski, A., Bono, G.: 2008, *Astron. Astrophys.*, 481, 441
- Hunt, J. A. S., Bub, M. W., Bovy, J., Mackereth, J. T., Trick, W. H., Kawata, D.: 2019, *Mon. Not. R. Astron. Soc.*, 490, 1026
- Leung, H. W., Bovy, J.: 2019, *Mon. Not. R. Astron. Soc.*, 489, 2079
- Lin, C. C., Shu, F. H.: 1964, *Astrophys. J.*, 140, 646
- Lin, C. C., Yuan, C., Shu, F. H.: 1969, *Astrophys. J.*, 155, 721
- Lindgren, L.: 2018, Gaia technical note GAIA-C3-TN-LU-LL-124, <https://www.cosmos.esa.int/web/gaia/ll-124>
- Lindgren, L., Hernández, J., Bombrun, A., et al.: 2018a, *Astron. Astrophys.*, 616, A2
- Lindgren, L., Hernández, J., Bombrun, A., et al. *Gaia DR2 astrometry*, report at IAU Symp. 30, Viena: 2018b, <https://www.cosmos.esa.int/web/gaia/dr2-known-issues#AstrometryConsiderations>
- Luri, X., Brown, A. G. A., Sarro, L. M., Arenou, F., Bailer-Jones, C. A. L., Castro-Ginard, A., de Bruijne, J., Prusti, T., Babusiaux, C., Delgado, H. E.: 2018, *Astron. Astrophys.*, 616, 9
- Melnik, A. M.: 2019, *Mon. Not. R. Astron. Soc.*, 485, 2106
- Melnik, A. M., Dambis, A. K.: 2009, *Mon. Not. R. Astron. Soc.*, 400, 518
- Melnik, A. M., Dambis, A. K.: 2017, *Mon. Not. R. Astron. Soc.*, 472, 3887
- Melnik, A. M., Dambis, A. K.: 2020, *Mon. Not. R. Astron. Soc.*, 2339
- Melnik, A. M., Rautiainen, P.: 2009, *Astron. Lett.* 35, 609
- Melnik, A. M., Rautiainen, P.: 2011, *Mon. Not. R. Astron. Soc.*, 418, 2508
- Melnik, A. M., Rautiainen, P., Berdnikov, L. N., Dambis, A. K., Rastorguev, A. S.: 2015, *AN* 336, 70
- Melnik, A. M., Rautiainen, P., Glushkova, E. V., Dambis, A. K.: 2016, *Astrophys. Space Sci.*, 361, 60
- Nikiforov, I. I.: 2004, *ASP Conf. Ser. Vol. 316*, *Astron. Soc. Pac.*, San Francisco, p. 199
- Ochsenbein, F., Bauer, P., Marcout, J.: 1997, *Astron. Astrophys. Suppl. Ser.*, 143, 23
- Pettitt, A. R., Ragan, S. E., Smith, M. C.: 2020, *Mon. Not. R. Astron. Soc.*, 491, 2162
- Rastorguev, A. S., Utkin, N. D., Zabolotskikh, M. V., Dambis, A. K., Bajkova, A. T., Bobylev, V. V.: 2017, *Astroph. Bull.* 72, 122
- Rautiainen, P., Melnik, A. M.: 2010, *Astron. Astrophys.*, 519, 70
- Reid, M. J., Menten, K. M., Zheng, X. W., Brunthaler, A., Xu, Y.: 2009, *Astrophys. J.*, 705, 1548
- Riess, A. G., et al.: 2018, *Astrophys. J.*, 861, 126
- Russeil, D.: 2003, *Astron. Astrophys.*, 397, 133
- Schönrich, R., Binney, J., Dehnen, W.: 2010, *Mon. Not. R. Astron. Soc.*, 403, 1829
- Schönrich, R., McMillan, P., Eyer, L.: 2019, *Mon. Not. R. Astron. Soc.*, 487, 3568
- Sitnik, T. G., Melnik, A. M.: 1996, *Astron. Lett.* 22, 422
- Stassun, K. G., Torres, G.: 2018, *Astrophys. J.*, 862, 61
- Tian, H.-J., Liu, C., Carlin, J., et al.: 2015, *Astrophys. J.*, 809, 145
- Vallée, J. P.: 2019, *Mon. Not. R. Astron. Soc.*, 489, 2819
- Yalyalieva, L. N., Chemel, A. A., Glushkova, E. V., Dambis, A. K., Klinichev, A. D.: 2018, *Astroph. Bull.* 73, 335
- Zinn, J. C., Pinsonneault, M. H., Huber, D., Stello, D.: 2019, *Astrophys. J.*, 878, 136